ACS APPLIED ENERGY MATERIALS

www.acsaem.org

Forum Article

Near-UV-to-Near-IR Hyperbolic Photonic Dispersion in Epitaxial (Hf,Zr)N/ScN Metal/Dielectric Superlattices

Prasanna Das, Krishna Chand Maurya, Jeremy L. Schroeder, Magnus Garbrecht, and Bivas Saha*

Cite This: https://doi.org/10.1021/acsaem.1c03467

Read Online

ACCESS | Metrics & More | Article Recommendations | Supporting Information

ABSTRACT: Hyperbolic metamaterials (HMMs) with extreme dielectric anisotropy have shown great promise in nanophotonic applications such as superlensing, enhancement of spontaneous emission, negative refraction, and the diverging photonic density of states. Noble metal-based metal/dielectric multilayers (e.g., Au/SiO_2 and Ag/TiO_2) and metallic (Au and Ag) nanowires embedded inside a dielectric matrix have been traditionally used to demonstrate HMM properties and for implementations into devices. Noble metals are, however, unstable at high temperatures, complementary metal oxide semiconductor incompatible, and difficult to deposit in thin-film form due to their high surface energies that limit their potential applications. TiN has emerged as an alternative plasmonic material to Au in recent years, and epitaxial TiN/$Al_{0.72}Sc_{0.28}N$ metal/semiconductor superlattices were developed that exhibit excellent HMM properties. As TiN exhibits ε-near-zero (ENZ) at ~500 nm, TiN/$Al_{0.72}Sc_{0.28}N$ HMM also operates from ~500 nm to long-wavelength regions. However, for several energy-conversion-related applications as well as for fundamental studies, it is desirable to achieve HMM wavelengths from the near-UV to the near-IR region of the spectrum. In this article, we demonstrate hyperbolic photonic dispersion in (Hf,Zr)N/ScN, a class of metal/semiconducting superlattice metamaterial that covers the near-UV to the near-IR spectral range. Epitaxial HfN/ScN, ZrN/ScN, and $Hf_{0.5}Zr_{0.5}N$/ScN superlattices are deposited on (001) MgO substrates and characterized with synchrotron-radiation X-ray diffraction as well as high-resolution electron microscopy techniques. Superlattices grow with cube-on-cube epitaxy and with sharp interfaces. Optical characterization reveals both type-I and type-II hyperbolic photonic dispersions as well as low losses and high figures-of-merit. Along with its high-temperature thermal stability, demonstration of HMM properties in (Hf,Zr)N/ScN metal/dielectric superlattices makes them potential candidates for HMM devices.

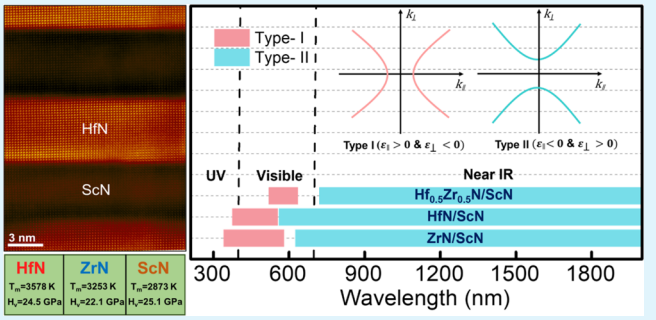

KEYWORDS: *hyperbolic metamaterials, transition metal nitrides, epitaxial metal/dielectric superlattice, magnetron sputtering, transmission electron microscopy*

1. INTRODUCTION

Optical metamaterials are artificial structures with subwavelength characteristics and exotic electromagnetic properties that are not observed in natural materials.[1−5] Among the various categories of optical metamaterials, hyperbolic metamaterials (HMMs) have drawn significant interest in recent years to achieve negative refraction,[6] subwavelength imaging,[7,8] enhancement of photonic density of states,[9−12] thermal emission engineering,[13] and others.[14−17] Extreme structural anisotropy in hyperbolic metamaterials (HMMs) results in hyperbolic photonic dispersion of their isofrequency surfaces, making them behave as metals in one direction and as a dielectric along the orthogonal directions.[18] Due to the isofrequency surface, unbounded wave vector, and divergent photonic densities of states, HMMs have attracted significant attention for the enhancement of spontaneous emission in single-photon sources,[19] thermal hyperconductivity,[20] hyperlenses,[21,22] waveguides,[23] and resonators.[9]

Most implementations of HMMs utilize metal/dielectric periodic multilayers/superlattices or metallic nanowires embedded inside a dielectric matrix.[24,25] Because their periodicity is much smaller than the wavelength of light, they act as an effective medium for light propagation and are described by anisotropic dielectric permittivity with opposite signs in the principal components of the dielectric tensor. Traditionally noble metal-based multilayers such as Au/Al_2O_3[26] and Ag/TiO_2[11] and metallic nanowires (Ag and Au) embedded inside dielectric hosts are utilized in device design.[27,28] Noble metals such as Ag and Au exhibit ε-near-

Special Issue: Early Career Forum

Received: November 5, 2021
Accepted: December 29, 2021

zero (ENZ) at ~390 and ~530 nm, respectively.[29] As a result, HMMs composed of Ag and Au exhibit hyperbolic dispersions starting from ~390 and ~530 nm, respectively, covering the full visible spectral range. However, noble metals are soft, unstable at high temperatures, and complementary metal oxide semiconductor (CMOS) incompatible as they diffuse into Si, leading to trapping states that reduce carrier lifetimes.[30] Prevention of such atom diffusion is necessary to grow epitaxial films on Si substrate, and efforts have been made to prevent atomic diffusion into Si by using different buffer layers.[31−33] But high surface energies (1−2 J/m^2) of noble metals lead to their higher surface roughness, which prevents their deposition in thin-film form essential for device implementations.[34] Therefore, high-quality CMOS compatible metal/dielectric superlattice HMMs are required that are not only structurally, chemically, and thermally stable but also demonstrate a broadband hyperbolic photonic dispersion with low losses.

Transition metal nitrides (TMNs) such as TiN have recently emerged as an alternative plasmonic material to Au for visible spectral range applications, and several plasmonic and thermoplasmonic devices based on TiN have been demonstrated.[35−40] Epitaxial TiN/$Al_{0.72}Sc_{0.28}N$ metal/semiconductor superlattices were developed that exhibit HMM properties in the visible-to-infrared spectral range and with an enhancement in the densities of photonic states.[41] However, TiN exhibits ENZ at ~500 nm, and as a result the hyperbolic photonic dispersion in TiN/$Al_{0.72}Sc_{0.28}N$ superlattices also starts at a similar wavelength.[42] As a result, hyperbolic dispersion and metamaterial properties in the blue-to-near-UV part of the electromagnetic spectrum have not been demonstrated in TMNs so far. HMMs that cover the full visible spectral range as well as near-UV and near-IR regions are however desirable for both fundamental studies and applications.

ZrN and HfN are similar TMNs like TiN and exhibit ENZs at ~340 and ~370 nm, respectively.[43,44] ZrN and HfN are corrosion-resistant, hard, and stable refractory TMNs and are used for hard coating applications.[45] Due to the long photoexcited carrier lifetime as high as a nanosecond, HfN has attracted interest for hot-carrier solar cell applications.[46] Similarly, due to its biocompatibility, ZrN-based coatings are also utilized in medical components that come into direct contact with blood, skin, bones, or tissue.[47] Therefore, nanoscale metal/dielectric superlattices with ZrN and HfN as metallic (plasmonic) components could lead to broadband HMM properties that should cover the full visible spectral range.

Sputter-deposited (Hf,Zr)N/ScN metal/semiconductor superlattices have been developed over the past few years and are currently explored for the thermionic emission-based thermoelectric energy conversion.[48] Because degenerate-semiconducting ScN is lattice-matched to HfN and exhibits less than 1% lattice mismatch with ZrN, (Hf, Zr)N/ScN superlattices exhibit sharp interfaces with an interatomic mixing of 2−3 unit cells.[49] Cross-plane transport measurements have demonstrated a Schottky barrier height of ~280 meV at the metal/semiconductor interfaces in ZrN/ScN superlattices.[48] Due to the presence of the Schottky barrier and filtering of low-energy electrons, ZrN/ScN superlattices have demonstrated a high Seebeck coefficient along the cross-plane directions.[50] Further efforts are also underway to develop thermionic emission devices with these metamaterials. In terms of thermal conduction, mismatches in the phononic density of states between the metallic HfN, ZrN with semiconducting ScN have also resulted in a much reduced cross-plane thermal conductivity in HfN/ScN, ZrN/ScN, and $Hf_{0.5}Zr_{0.5}N$/ScN superlattices compared to the individual nitride materials.[51,52]

High-temperature thermal stability analyses have further demonstrated that (Hf,Zr)N/ScN superlattices are stable up to 850 °C.[49] At high temperatures, dislocation pipe diffusion of Hf and/or Zr atoms along threading dislocations is observed.[53] In summary, significant research efforts have been already directed toward the development and study of the thermionic, electronic, and thermal transport properties of (Hf,Zr)N/ScN metal/semiconductor superlattices and to analyze their thermal stability. In this article, we report on the optical HMM properties of (Hf,Zr)N/ScN metal/dielectric superlattices and show that the hyperbolic photonic dispersion covers the full visible spectral range as well as near-UV and near-IR regions.

2. EXPERIMENTAL DETAILS

Individual HfN, ZrN, $Hf_{0.5}Zr_{0.5}N$, and ScN thin films and 6 nm/6 nm HfN/ScN, ZrN/ScN, and $Hf_{0.5}Zr_{0.5}N$/ScN metal/semiconductor superlattices with a period thickness of 12 nm are deposited on MgO substrate with DC-magnetron sputtering inside an ultrahigh-vacuum chamber with a base pressure of 1×10^{-8} Torr at a growth temperature of 850 °C. Because MgO exhibits the same rock-salt crystal structure as the nitrides, (001) MgO substrates are utilized for the superlattice growth. The structural quality of the superlattices is determined with synchrotron-radiation high-resolution X-ray diffraction in the High Energy Materials Science beamline PETRA 07 of the DESY (Hamburg, Germany) and with high-resolution scanning transmission electron microscopy (HR(S)/TEM) studies. The optical properties of individual thin films and the superlattices are measured with a spectroscopic ellipsometer from the 210 to 2000 nm range. Details about the growth and characterization techniques are presented in the Supporting Information (SI).

3. RESULTS AND DISCUSSION

3.1. Structural Characterization. *Synchrotron-Radiation High-Resolution X-ray Diffraction.* A schematic of the synchrotron-radiation X-ray diffraction measurement (see Figure 1a) shows that the experiments were conducted in the transmission mode by directing the X-ray beam of ~10 × 400 μm approximately parallel to the sample surface.[54] The beam was approximately parallel to the (001) MgO substrate, and the substrate was also partially illuminated with the X-ray beam. But due to the intentional misalignment of the substrate with respect to the X-ray beam, little-to-no signal was observed from the MgO (see SI for details). Two-dimensional (2D) X-ray diffraction patterns of the HfN/ScN (Figure 1b), ZrN/ScN (Figure 1c), and $Hf_{0.5}Zr_{0.5}N$/ScN (Figure 1d) superlattices deposited on (001) MgO substrates show (002) oriented growth as evidenced by the 002 reflections, which are oriented along the growth direction. Corresponding to the diffraction peaks from the {002} family of planes *d*-spacings of 2.26 Å for HfN/ScN, 2.29 Å for ZrN/ScN, and 2.27 Å for $Hf_{0.5}Zr_{0.5}N$/ScN superlattices are measured, corresponding to cross-plane lattice constants of 4.52, 4.58, and 4.54 Å, respectively. As individual HfN, ZrN, $Hf_{0.5}Zr_{0.5}N$, and ScN films exhibit lattice constants of 4.52, 4.59, 4.55, and 4.52 Å, respectively, the cross-plane lattice constants are close to the average values of the individual layers.[51] Superlattice reflections are also clearly visible in all of the diffraction patterns, which are indicative of sharp interfaces. Previous laboratory-source X-ray diffraction has shown that the superlattices are epitaxial in nature in all cases. From the interference pattern, a period thickness of 11.3 nm is measured that matches well with the growth target and

https://doi.org/10.1021/acsaem.1c03467
ACS Appl. Energy Mater. XXXX, XXX, XXX−XXX

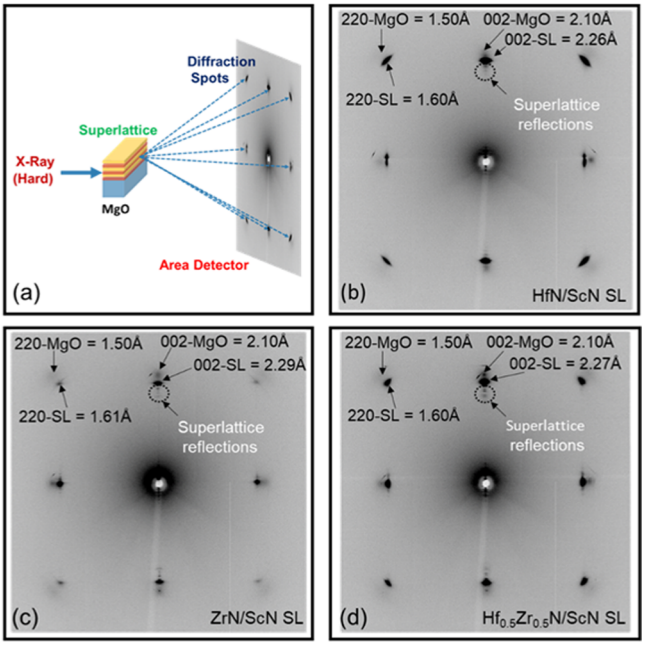

Figure 1. (a) Schematic of synchrotron-radiation 2D X-ray diffraction imaging of superlattice in transmission mode. Diffraction patterns of (b) HfN/ScN, (c) ZrN/ScN, and (d) $Hf_{0.5}Zr_{0.5}N$/ScN superlattices are presented. All of the superlattices are (002) oriented on (001) MgO substrates. Sharp interfaces in superlattices produce the superlattice reflections in each case.

HR(S)/TEM analysis.[55] Faint MgO 002 diffraction spots from {002} planes with a *d*-spacing of 2.1 Å can be seen in each of the images, corresponding to a bulk MgO lattice constant of 4.20 Å.

High-Resolution (Scanning)/Transmission Electron Microscopy. A low-magnification STEM image (see Figure 2a) of an $Hf_{0.5}Zr_{0.5}N$/ScN superlattice shows the superlattice layer growth on the $Hf_{0.5}Zr_{0.5}N$/MgO buffer/substrate layer. The interface between the superlattice and bottom metallic buffer layer ($Hf_{0.5}Zr_{0.5}N$ in this case) is sharp within a width of 2−3 unit cells. However, due to a ∼7% lattice-mismatch between the (001) MgO substrate and the nitride layers, threading dislocations are observed, and the layers appear wavy with periods of 100−200 nm. An atomic-resolution STEM image of the $Hf_{0.5}Zr_{0.5}N$/ScN interface (Figure 2b) shows cubic epitaxial growth with an orientation relationship of (001) [001] $Hf_{0.5}Zr_{0.5}N$/ScN||(001) [001] MgO (see inset electron diffraction pattern Figure 2a). The combined energy-dispersive X-ray spectroscopy (EDS) mapping (see Figure 2c), as well as individual EDS maps of Hf (see Figure 2d), Sc (see Figure 2e), and Zr (see Figure 2f) show a slight broadening of the Zr layer.

3.2. Optical Characterization. Dielectric permittivities of individual nitride thin films (HfN, ZrN, and ScN) and the alloy ($Hf_{0.5}Zr_{0.5}N$) film measured with spectroscopic ellipsometry are presented in Figure 3. Results show that HfN, ZrN, and $Hf_{0.5}Zr_{0.5}N$ exhibit a real component of the dielectric permittivity (ϵ') positive-to-negative crossover at 370, 340, and 490 nm, respectively (see Figure 3a). Such a crossover or ϵ-near-zero (ENZ) is representative of the onset of their metallic character. At the crossover wavelength, the imaginary parts of dielectric permittivity (ϵ''; see Figure 3b) are 1.6, 1.8, and 3.2, respectively, for the HfN, ZrN, and $Hf_{0.5}Zr_{0.5}N$ films, which are comparable to well-known noble metal-based plasmonic materials such as Au and Ag, as well as with

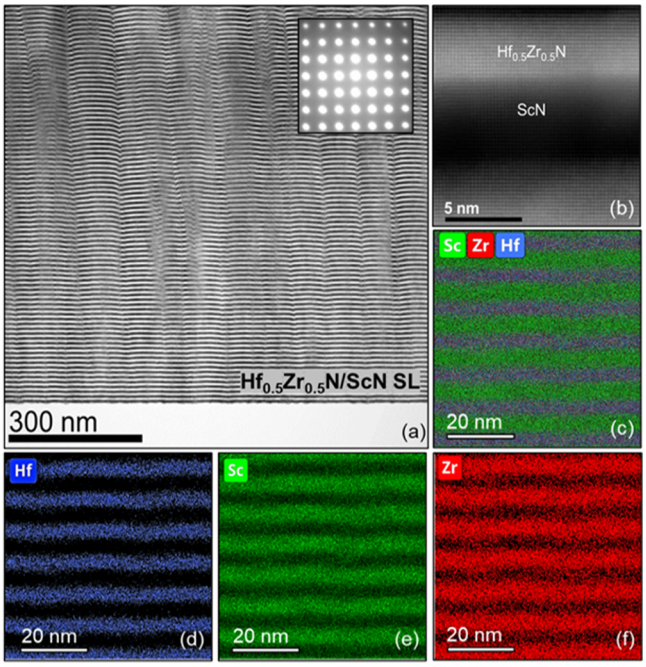

Figure 2. (a) Low-magnification, high-angle annular dark-field (HAADF)-STEM micrograph of a $Hf_{0.5}Zr_{0.5}N$/ScN superlattice deposited on a $Hf_{0.5}Zr_{0.5}N$ buffer layer on (001) MgO substrate. The electron diffraction pattern of the superlattice is presented in the inset. (b) High-resolution image showing that $Hf_{0.5}Zr_{0.5}N$ and ScN layers are grown heteroepitaxial. (c) Combined STEM−energy-dispersive X-ray spectroscopy and (d−f) individual element maps.

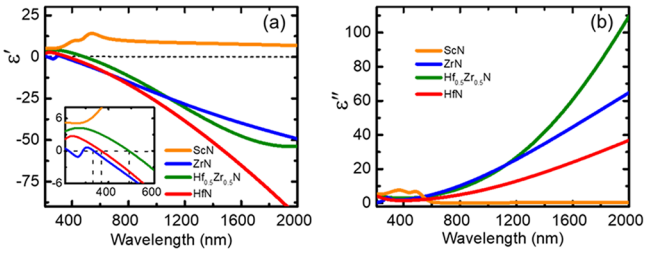

Figure 3. (a) Real and (b) imaginary parts of dielectric permittivity (measured with spectroscopic ellipsometry) of the constituent layers (HfN, ZrN, $Hf_{0.5}Zr_{0.5}N$, and ScN) of the superlattices. The inset in panel a zooms into the wavelength range 210−600 nm, which suggests that the ENZ wavelengths of HfN, ZrN, and $Hf_{0.5}Zr_{0.5}N$ are 370, 340, and 490 nm, respectively.

TiN.[29,36] It is interesting to note that both HfN and ZrN exhibit an ENZ wavelength comparable to Ag[29] but much smaller than those of TiN and Au.[29,44,56] Therefore, for many near-UV-to-blue spectral applications or for devices where full visible spectra need to be accessed, both HfN and ZrN can be considered as an alternative plasmonic material to Ag. After the crossover wavelength, the magnitudes of the ϵ' in all three metals increase with an increase in the wavelength. HfN exhibits the largest negative ϵ' followed by the $Hf_{0.5}Zr_{0.5}N$ alloy and ZrN film. The ENZ wavelength of the $Hf_{0.5}Zr_{0.5}N$ alloy is higher among the three nitrides possibly due to higher alloy scattering of carriers that reduces the mobility. The magnitude of ϵ' of all three metals is, in general, lower than those of noble metals (Ag and Au).

Compared to the metals, ScN exhibits (see Figure 3a) a dielectric optical characteristic consistent with its semi-

https://doi.org/10.1021/acsaem.1c03467
ACS Appl. Energy Mater. XXXX, XXX, XXX−XXX

conducting nature with a direct band gap of 2.2 eV.[57] Near the band gap region, the ϵ' of ScN exhibits a maximum value of 14.2, which is close to Si's ϵ^{∞} of 11.7.[58] It is important to note here that ScN exhibits an indirect band gap of ∼0.9 eV that is close to the indirect band gap of Si (1.1 eV). At longer wavelengths, ϵ' in ScN is nearly constant at 6. Because ScN is a degenerate semiconductor,[59] at long wavelengths (in the near-IR spectral regions) optical loss or ϵ'' increases due to free electron or Drude contributions. Nevertheless, ϵ'' of ScN at long-wavelength regions (see Figure 3b) is much smaller compared to the optical loss of the metals.

Having determined the optical properties of the individual thin films, ellipsometry measurements are used to measure and calculate the optical properties of the superlattices. Because superlattices are anisotropic in nature, the total dielectric permittivity exhibits both in-plane ($\epsilon_{||}$) and out-of-plane ($\epsilon_{\perp}$) components. Ellipsometry data fitting-derived dielectric permittivity of the individual layers is used in the effective medium theory (see the SI) to calculate the permittivity of the superlattices.[60] Results show that, in general, all three superlattices exhibit similar HMM properties. HfN/ScN superlattices exhibit (Figure 4a,b) type-I hyperbolic dispersion

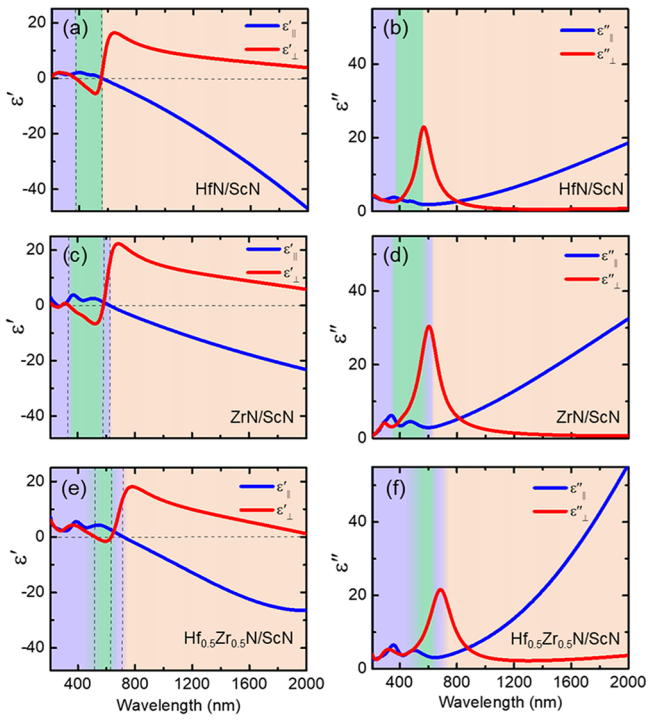

Figure 4. Real and imaginary components of the effective permittivities for the HfN/ScN (a and b), ZrN/ScN (c and d), and $Hf_{0.5}Zr_{0.5}N$/ScN (e and f) superlattices. In-plane and out-of-plane directions have been represented by blue and red lines, respectively. Three different regions—elliptical (violet), hyperbolic type-I (green), and hyperbolic type-II (orange)—are represented by the three different background colors. All three superlattices exhibit both type-I and type-II hyperbolic dispersion.

(characterized by $\epsilon'_{\perp} < 0$ and $\epsilon'_{||} > 0$) from 375 to 560 nm and type-II hyperbolic dispersion (characterized by $\epsilon'_{\perp} > 0$ and $\epsilon'_{||} < 0$) from 560 to 2000 nm. Below the ENZ of HfN at 370 nm, HfN/ScN superlattices are found to exhibit dielectric optical behavior (characterized with $\epsilon'_{\perp} > 0$ and $\epsilon'_{||} > 0$), as expected. Consistent with the HMM properties, $\epsilon''_{\perp}$ also exhibits a Gaussian-like sharp peak centered at the type-I to type-II crossover wavelength of 560 nm. $\epsilon''_{||}$ of the superlattice increases with an increase in the wavelength. The inclusion of dielectric layers between the HfN layers dilutes its metallic characteristics, evidenced by the higher $\epsilon'_{||}$ crossover wavelength to 560 nm and lower values of $\epsilon'_{||}$ at higher wavelengths compared to an HfN thin film. Similarly, a decrease in the $\epsilon'_{\perp}$ with an increase in the wavelength is due to the onset of Drude absorption in ScN layers due to its high carrier densities in the $(2-5) \times 10^{20}$ cm^{-3} range.

Similar to HfN/ScN, ZrN/ScN superlattices (see Figure 4c,d) exhibit type-I hyperbolic dispersion from 340 to 580 nm and type-II hyperbolic dispersion from 625 to 2000 nm. However, unlike HfN/ScN superlattices, there is a small spectral range between 580 and 625 nm where both $\epsilon'_{||}$ and $\epsilon'_{\perp}$ are positive and the photonic dispersion should be elliptical. Below the ENZ point of ZrN, ZrN/ScN superlattices also exhibit dielectric characteristics. Panels e and f of Figure 4 show that the HMM properties of the $Hf_{0.5}Zr_{0.5}N$/ScN superlattices are very similar to ZrN/ScN superlattices, albeit a lower window for the type-I hyperbolic dispersion. Similar to the other two superlattices, $\epsilon''_{\perp}$ of $Hf_{0.5}Zr_{0.5}N$/ScN superlattices shows a Gaussian peak around ∼700 nm. However, unlike HfN/ScN and ZrN/ScN superlattices, $\epsilon''_{\perp}$ increases slightly after 1200 nm due to a higher amount of free carrier absorption in $Hf_{0.5}Zr_{0.5}N$/ScN superlattices. Therefore, the present analysis clearly demonstrates both type-I and type-II hyperbolic photonic dispersions in the (Hf,Zr)N/ScN metal/dielectric superlattices with the type-I region starting from as low as ∼340 nm, what would allow the material to cover the near-UV to the entire visible and near-IR spectral range.

Angle-dependent reflection (R) measurements of the superlattices and theoretical calculations further verify the hyperbolic photonic dispersion of the superlattices. Figure 5

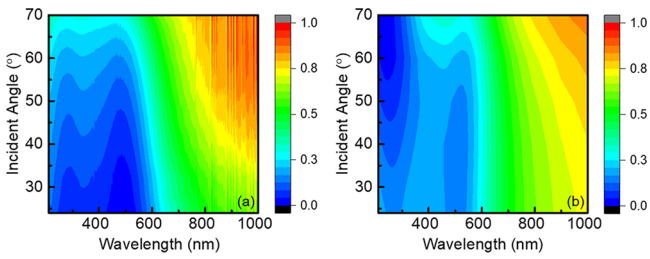

Figure 5. (a) Reflection spectrum of 6 nm/6 nm HfN/ScN superlattice presented as a function of incident angle (measured using spectroscopic ellipsometry). (b) Theoretically calculated reflection spectra of the same superlattice (using COMSOL Multiphysics Software) that indicates a clear match up with experimentally measured spectrum.

presents reflection curves for the HfN/ScN superlattice, and these curves are also representative for the other two superlattices. At longer wavelengths, since the superlattices act as type-II HMM, high reflectivity is observed in both experiment and the modeling. However, because the wavelength is reduced, two dips in the reflection spectra at ∼290 and ∼485 nm are observed that correspond to the $\epsilon'_{||}$ of the superlattice approaching ENZ and HfN's inherent crossover wavelength or ENZ points.

Figure-of-merit (FOM) calculations are further carried out to determine the performance of the (Hf,Zr)N/ScN superlattice HMMs and compare their performance to each other as

https://doi.org/10.1021/acsaem.1c03467
ACS Appl. Energy Mater. XXXX, XXX, XXX−XXX

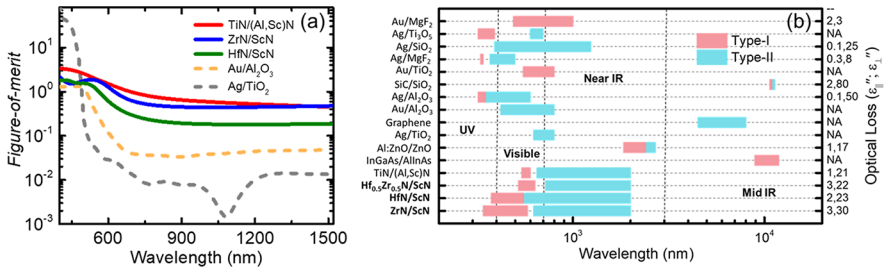

Figure 6. (a) Figures-of-merit (FOMs) of HfN/ScN and ZrN/ScN superlattices presented along with TiN/(Al, Sc)N and noble metal-based multilayers such as Ag/TiO_2 and Au/Al_2O_3. (b) Hyperbolic wavelength bands for various metal/dielectric multilayers. Type-I (orange) and type-II (turquoise green) hyperbolic bands are denoted by color. (Hf,Zr)N/ScN superlattices have been compared with the earlier reported metal/dielectric multilayers.[11,26,74,41,67−73] The right-hand-side *y*-scale represents the maximum optical loss (calculated at type-I to type-II crossover wavelength) along in-plane and out-of-plane directions.

well as to other HMMs in different spectral ranges. The FOM is usually defined as $\frac{\mathrm{Re}(k_\perp)}{\mathrm{Im}(k_\perp)}$, the ratio between the real and imaginary components of the propagation constant of light (k) in the direction perpendicular to the constituent layers.[42] Figure 6a shows that compared to the Ag/TiO_2 and Au/Al_2O_3 HMMs, HfN/ScN and ZrN/ScN superlattices exhibit about 10 times higher FOMs in the long-wavelength spectral range.[26,61] However, in the blue-to-near-UV parts of the spectrum, the FOMs of Au/Al_2O_3 HMM and TMN-based HMM are very similar, while the FOM of Ag/TiO_2 HMMs is higher. Therefore, for practical applications where high-temperature stability, corrosion-resistant high-hardness, CMOS compatibility, etc., are important design parameters, HfN/ScN and ZrN/ScN HMMs would provide a meaningful alternative materials choice. It is also interesting to note that the FOM of ZrN/ScN superlattices is much closer to the FOM of TiN/$Al_{0.72}Sc_{0.28}N$ superlattices.

A comparative plot of the hyperbolic dispersion frequency range and the optical loss (see Figure 6b) highlights that, with the development of (Hf,Zr)N/ScN superlattice HMMs, the entire near-UV-to-visible-to-near-IR region of the spectrum can be covered with TMN-based materials. While previously it was only possible to achieve hyperbolic dispersion in the blue-to-near-UV region of the spectrum with Ag as a metallic component, HfN and ZrN now allow access to a larger spectral range. Though the optical losses are higher in TMN-based HMMs compared to the noble metal-based HMMs, their high-temperature stability, corrosion-resistant high hardness, and structural/morphological stability in the thin-film form make them attractive for practical applications. In addition, the wide-spectral coverage of these materials will not only be useful for the solid-state energy conversion fields such as solar−thermal,[62] and solar−fuel,[63] they will also be attractive for biophotonics,[64] sensing,[65] and illumination nanoscopy.[66]

4. CONCLUSIONS

In conclusion, we extend the spectral operation range of the transition metal nitride (TMN)-based hyperbolic metamaterials by developing epitaxial (Hf,Zr)N/ScN metal/semiconductor superlattice HMMs. Our results show nanoscale HfN/ScN, ZrN/ScN, and $Hf_{0.5}Zr_{0.5}N$/ScN metal/semiconductor superlattices exhibit both type-I and type-II hyperbolic photonic dispersions starting from ∼340 nm covering the blue and near-UV spectral range. Achieving the HMM dispersion in the blue-to-near-UV region provides an alternative to Ag-based HMMs. The figure-of-merit of these HMMs is also found to be high. Synchrotron-radiation high-resolution X-ray diffraction and high-resolution (scanning)/ transmission electron microscopy analyses are performed to demonstrate cubic epitaxial crystal growth on (001) MgO substrates. Demonstration of hyperbolic photonic dispersion from near-UV to near-IR spectral range in (Hf,Zr)N/ScN metal/semiconductor superlattices mark significant progress in designing refractory, CMOS-compatible artificially structured nanophotonic materials that should be useful for practical applications.

■ ASSOCIATED CONTENT

Supporting Information

The Supporting Information is available free of charge at https://pubs.acs.org/doi/10.1021/acsaem.1c03467.

Details on growth, STEM-EDS mapping, synchrotron-radiation X-ray diffraction, ellipsometer measurements, effective medium theory, and figure-of-merit calculation (PDF)

■ AUTHOR INFORMATION

Corresponding Author

Bivas Saha − *Chemistry and Physics of Materials Unit, International Centre for Materials Science, and School of Advanced Materials, Jawaharlal Nehru Centre for Advanced Scientific Research, Bangalore 560064, India;* orcid.org/0000-0002-0837-1506; Email: bsaha@jncasr.ac.in, bivas.mat@gmail.com

Authors

Prasanna Das − *Chemistry and Physics of Materials Unit and International Centre for Materials Science, Jawaharlal Nehru Centre for Advanced Scientific Research, Bangalore 560064, India*

Krishna Chand Maurya − *Chemistry and Physics of Materials Unit and International Centre for Materials Science, Jawaharlal Nehru Centre for Advanced Scientific Research, Bangalore 560064, India*

Jeremy L. Schroeder − *Thin Film Physics Division, Department of Physics, Chemistry, and Biology (IFM), Linköping University, 581 83 Linköping, Sweden*

Magnus Garbrecht − *Australian Centre for Microscopy and Microanalysis, The University of Sydney, Camperdown, New South Wales 2006, Australia*

Complete contact information is available at: https://pubs.acs.org/10.1021/acsaem.1c03467

Notes

The authors declare no competing financial interest.
Data available on request from the authors.

■ ACKNOWLEDGMENTS

P.D., K.C.M., and B.S. acknowledge the International Centre for Materials Science (ICMS) and Sheikh Saqr Laboratory (SSL) in JNCASR for support. B.S. acknowledges the Ras Al Khaimah Centre for Advanced Materials and Raknor LLC for financial support. M.G. acknowledges the facilities of Sydney Microscopy and Microanalysis at The University of Sydney. J.L.S. acknowledges Dr. Norbert Schell for helping in synchrotron-radiation X-ray diffraction at DESY, Hamburg. P.D. and K.C.M. thank the Council of Scientific & Industrial Research (CSIR) for a fellowship.

■ REFERENCES

(1) Pendry, J. B.; Schurig, D.; Smith, D. R. Controlling Electromagnetic Fields. *Science.* **2006**, *312* (5781), 1780−1782.
(2) Shalaev, V. M. Transforming Light. *Science.* **2008**, *322* (5900), 384−386.
(3) Ivinskaya, A.; Kostina, N.; Proskurin, A.; Petrov, M. I.; Bogdanov, A. A.; Sukhov, S.; Krasavin, A. V.; Karabchevsky, A.; Shalin, A. S.; Ginzburg, P. Optomechanical Manipulation with Hyperbolic Metasurfaces. *ACS Photonics* **2018**, *5* (11), 4371−4377.
(4) Kostina, N. A.; Kislov, D. A.; Ivinskaya, A. N.; Proskurin, A.; Redka, D. N.; Novitsky, A.; Ginzburg, P.; Shalin, A. S. Nanoscale Tunable Optical Binding Mediated by Hyperbolic Metamaterials. *ACS Photonics* **2020**, *7* (2), 425−433.
(5) Kim, M.; Lee, D.; Kim, T. H.; Yang, Y.; Park, H. J.; Rho, J. Observation of Enhanced Optical Spin Hall Effect in a Vertical Hyperbolic Metamaterial. *ACS Photonics* **2019**, *6* (10), 2530−2536.
(6) Shalaev, V. M. Optical Negative-Index Metamaterials. *Nat. Photonics* **2007**, *1* (1), 41−48.
(7) Liu, Z.; Lee, H.; Xiong, Y.; Sun, C.; Zhang, X. Far-Field Optical Hyperlens Magnifying Sub-Diffraction-Limited Objects. *Science.* **2007**, *315* (5819), 1686−1686.
(8) Qian, C.; Lin, X.; Yang, Y.; Gao, F.; Shen, Y.; Lopez, J.; Kaminer, I.; Zhang, B.; Li, E.; Soljačić, M.; Chen, H. Multifrequency Superscattering from Subwavelength Hyperbolic Structures. *ACS Photonics* **2018**, *5* (4), 1506−1511.
(9) Feng, K.; Harden, G.; Sivco, D. L.; Hoffman, A. J. Subdiffraction Confinement in All-Semiconductor Hyperbolic Metamaterial Resonators. *ACS Photonics* **2017**, *4* (7), 1621−1626.
(10) Jacob, Z.; Kim, J.-Y.; Naik, G. V.; Boltasseva, A.; Narimanov, E. E.; Shalaev, V. M. Engineering Photonic Density of States Using Metamaterials. *Appl. Phys. B: Laser Opt.* **2010**, *100* (1), 215−218.
(11) Krishnamoorthy, H. N. S.; Jacob, Z.; Narimanov, E.; Kretzschmar, I.; Menon, V. M. Topological Transitions in Metamaterials. *Science.* **2012**, *336* (6078), 205−209.
(12) Adl, H. P.; Gorji, S.; Habil, M. K.; Suárez, I.; Chirvony, V. S.; Gualdrón-Reyes, A. F.; Mora-Seró, I.; Valencia, L. M.; de la Mata, M.; Hernández-Saz, J.; Molina, S. I.; Zapata-Rodríguez, C. J.; Martínez-Pastor, J. P. Purcell Enhancement and Wavelength Shift of Emitted Light by CsPbI 3 Perovskite Nanocrystals Coupled to Hyperbolic Metamaterials. *ACS Photonics* **2020**, *7* (11), 3152−3160.
(13) Sohr, P.; Ip, C. I.; Law, S. Far-Field Thermal Emission from a Semiconductor Hyperbolic Metamaterial. *Opt. Lett.* **2019**, *44* (5), 1138.
(14) Yin, L.-Z.; Han, F.-Y.; Zhao, J.; Wang, D.; Huang, T.-J.; Liu, P.-K. Constructing Hyperbolic Metamaterials with Arbitrary Medium. *ACS Photonics* **2021**, *8* (4), 1085−1096.
(15) Maurya, K. C.; Bhui, A.; Biswas, K.; Saha, B. Anisotropic Epsilon-near-Pole (ENP) Resonance Leads to Hyperbolic Photonic Dispersion in Homologous (Bi 2) m (Bi 2 Se 3) n Topological Quantum Materials. *Appl. Phys. Lett.* **2021**, *119* (1), 011902.
(16) Poddubny, A.; Iorsh, I.; Belov, P.; Kivshar, Y. Hyperbolic Metamaterials. *Nat. Photonics* **2013**, *7* (12), 948−957.
(17) Ferrari, L.; Wu, C.; Lepage, D.; Zhang, X.; Liu, Z. Hyperbolic Metamaterials and Their Applications. *Prog. Quantum Electron.* **2015**, *40* (2014), 1−40.
(18) Smith, D. R.; Schurig, D. Electromagnetic Wave Propagation in Media with Indefinite Permittivity and Permeability Tensors. *Phys. Rev. Lett.* **2003**, *90* (7), 077405.
(19) Cortes, C. L.; Newman, W.; Molesky, S.; Jacob, Z. Corrigendum: Quantum Nanophotonics Using Hyperbolic Metamaterials (2012 J. Opt. 14 063001). *J. Opt.* **2014**, *16* (12), 129501.
(20) Narimanov, E.; Smolyaninov, I. Beyond Stefan-Boltzmann Law: Thermal Hyper-conductivity. In *2012 Conference on Lasers and Electro-Optics (CLEO)*; IEEE, 2012; p QM2E.1. DOI: 10.1364/QELS.2012.QM2E.1.
(21) Sun, J.; Xu, T.; Litchinitser, N. M. Experimental Demonstration of Demagnifying Hyperlens. *Nano Lett.* **2016**, *16* (12), 7905−7909.
(22) Jacob, Z.; Alekseyev, L. V.; Narimanov, E. Optical Hyperlens: Far-Field Imaging beyond the Diffraction Limit. *Opt. Express* **2006**, *14* (18), 8247.
(23) Roth, D. J.; Krasavin, A. V.; Wade, A.; Dickson, W.; Murphy, A.; Kéna-Cohen, S.; Pollard, R.; Wurtz, G. A.; Richards, D.; Maier, S. A.; Zayats, A. V. Spontaneous Emission inside a Hyperbolic Metamaterial Waveguide. *ACS Photonics* **2017**, *4* (10), 2513−2521.
(24) Maas, R.; van de Groep, J.; Polman, A. Planar Metal/Dielectric Single-Periodic Multilayer Ultraviolet Flat Lens. *Optica* **2016**, *3* (6), 592.
(25) Elser, J.; Wangberg, R.; Podolskiy, V. A.; Narimanov, E. E. Nanowire Metamaterials with Extreme Optical Anisotropy. *Appl. Phys. Lett.* **2006**, *89* (26), 261102.
(26) Sreekanth, K. V.; Biaglow, T.; Strangi, G. Directional Spontaneous Emission Enhancement in Hyperbolic Metamaterials. *J. Appl. Phys.* **2013**, *114* (13), 134306.
(27) Baqir, M. A.; Choudhury, P. K.; Mughal, M. J. Gold Nanowires-Based Hyperbolic Metamaterial Multiband Absorber Operating in the Visible and Near-Infrared Regimes. *Plasmonics* **2019**, *14* (2), 485−492.
(28) Baqir, M. A.; Choudhury, P. K. Toward Filtering Aspects of Silver Nanowire-Based Hyperbolic Metamaterial. *Plasmonics* **2018**, *13* (6), 2015−2020.
(29) Johnson, P. B.; Christy, R. W. Optical Constants of the Noble Metals. *Phys. Rev. B* **1972**, *6* (12), 4370−4379.
(30) Bemski, G. Recombination Properties of Gold in Silicon. *Phys. Rev.* **1958**, *111* (6), 1515−1518.
(31) Hassan, S. S. A.; Xu, Y.; Wu, J.; Thompson, S. M. Epitaxial Growth and Magnetic Properties of Half-Metallic Fe_3O_4 on Si(100) Using MgO Buffer Layer. *IEEE Trans. Magn.* **2009**, *45* (10), 4357−4359.
(32) Xiang, H.; Shi, F.; Rzchowski, M. S.; Voyles, P. M.; Chang, Y. A. Epitaxial Growth and Magnetic Properties of Fe3O4 Films on TiN Buffered Si(001), Si(110), and Si(111) Substrates. *Appl. Phys. Lett.* **2010**, *97* (9), 092508.
(33) Ishibe, T.; Maeda, Y.; Terada, T.; Naruse, N.; Mera, Y.; Kobayashi, E.; Nakamura, Y. Resistive Switching Memory Performance in Oxide Hetero-Nanocrystals with Well-Controlled Interfaces. *Sci. Technol. Adv. Mater.* **2020**, *21* (1), 195−204.
(34) Skriver, H. L.; Rosengaard, N. M. Surface Energy and Work Function of Elemental Metals. *Phys. Rev. B* **1992**, *46* (11), 7157−7168.
(35) Naik, G. V.; Shalaev, V. M.; Boltasseva, A. Alternative Plasmonic Materials: Beyond Gold and Silver. *Adv. Mater.* **2013**, *25* (24), 3264−3294.
(36) Naik, G. V.; Schroeder, J. L.; Ni, X.; Kildishev, A. V.; Sands, T. D.; Boltasseva, A. Titanium Nitride as a Plasmonic Material for Visible and Near-Infrared Wavelengths. *Opt. Mater. Express* **2012**, *2* (4), 478.
(37) Hibbins, A. P.; Sambles, J. R.; Lawrence, C. R. Surface Plasmon-Polariton Study of the Optical Dielectric Function of Titanium Nitride. *J. Mod. Opt.* **1998**, *45* (10), 2051−2062.

https://doi.org/10.1021/acsaem.1c03467
ACS Appl. Energy Mater. XXXX, XXX, XXX−XXX

(38) Maurya, K. C.; Shalaev, V. M.; Boltasseva, A.; Saha, B. Reduced Optical Losses in Refractory Plasmonic Titanium Nitride Thin Films Deposited with Molecular Beam Epitaxy. *Opt. Mater. Express* **2020**, *10* (10), 2679.
(39) Gadalla, M. N.; Chaudhary, K.; Zgrabik, C. M.; Capasso, F.; Hu, E. L. Imaging of Surface Plasmon Polaritons in Low-Loss Highly Metallic Titanium Nitride Thin Films in Visible and Infrared Regimes. *Opt. Express* **2020**, *28* (10), 14536.
(40) Garbrecht, M.; Hultman, L.; Fawey, M. H.; Sands, T. D.; Saha, B. Tailoring of Surface Plasmon Resonances in TiN/(Al0.72Sc0.28)N Multilayers by Dielectric Layer Thickness Variation. *J. Mater. Sci.* **2018**, *53* (6), 4001−4009.
(41) Naik, G. V.; Saha, B.; Liu, J.; Saber, S. M.; Stach, E. A.; Irudayaraj, J. M. K.; Sands, T. D.; Shalaev, V. M.; Boltasseva, A. Epitaxial Superlattices with Titanium Nitride as a Plasmonic Component for Optical Hyperbolic Metamaterials. *Proc. Natl. Acad. Sci. U. S. A.* **2014**, *111* (21), 7546−7551.
(42) Saha, B.; Naik, G. V.; Saber, S.; Akatay, C.; Stach, E. A.; Shalaev, V. M.; Boltasseva, A.; Sands, T. D. TiN/(Al,Sc)N Metal/Dielectric Superlattices and Multilayers as Hyperbolic Metamaterials in the Visible Spectral Range. *Phys. Rev. B* **2014**, *90* (12), 125420.
(43) Pilloud, D.; Dehlinger, A. S.; Pierson, J. F.; Roman, A.; Pichon, L. Reactively Sputtered Zirconium Nitride Coatings: Structural, Mechanical, Optical and Electrical Characteristics. *Surf. Coat. Technol.* **2003**, *174*−*175* (1), 338−344.
(44) Strømme, M.; Karmhag, R.; Ribbing, C. G. Optical Constants of Sputtered Hafnium Nitride Films. Intra- and Interband Contributions. *Opt. Mater. (Amst).* **1995**, *4* (5), 629−639.
(45) Acharya, S.; Saha, B. Epitaxial Nitride Thin Film and Heterostructures: From Hard Coating to Solid State Energy Conversion. In *Coatings and Thin-Film Technologies*, Perez-Taborda, J. A.; Bernal, A. G. A., Eds. IntechOpen, 2019. DOI: 10.5772/intechopen.79525.
(46) Chung, S.; Shrestha, S.; Wen, X.; Feng, Y.; Gupta, N.; Xia, H.; Yu, P.; Tang, J.; Conibeer, G. Hafnium Nitride for Hot Carrier Solar Cells. *Sol. Energy Mater. Sol. Cells* **2016**, *144* (March), 781−786.
(47) Kumar, D. D.; Kaliaraj, G. S. Multifunctional Zirconium Nitride/Copper Multilayer Coatings on Medical Grade 316L SS and Titanium Substrates for Biomedical Applications. *J. Mech. Behav. Biomed. Mater.* **2018**, *77*, 106−115.
(48) Saha, B.; Sands, T. D.; Waghmare, U. V. First-Principles Analysis of ZrN/ScN Metal/Semiconductor Superlattices for Thermoelectric Energy Conversion. *J. Appl. Phys.* **2011**, *109* (8), 083717.
(49) Garbrecht, M.; Schroeder, J. L.; Hultman, L.; Birch, J.; Saha, B.; Sands, T. D. Microstructural Evolution and Thermal Stability of HfN/ScN, ZrN/ScN, and Hf0.5Zr0.5N/ScN Metal/Semiconductor Superlattices. *J. Mater. Sci.* **2016**, *51* (17), 8250−8258.
(50) Zebarjadi, M.; Bian, Z.; Singh, R.; Shakouri, A.; Wortman, R.; Rawat, V.; Sands, T. Thermoelectric Transport in a ZrN/ScN Superlattice. *J. Electron. Mater.* **2009**, *38* (7), 960−963.
(51) Saha, B.; Acharya, J.; Sands, T. D.; Waghmare, U. V. Electronic Structure, Phonons, and Thermal Properties of ScN, ZrN, and HfN: A First-Principles Study. *J. Appl. Phys.* **2010**, *107* (3), 033715.
(52) Rawat, V.; Koh, Y. K.; Cahill, D. G.; Sands, T. D. Thermal Conductivity of (Zr,W)N/ScN Metal/Semiconductor Multilayers and Superlattices. *J. Appl. Phys.* **2009**, *105* (2), 024909.
(53) Garbrecht, M.; Saha, B.; Schroeder, J. L.; Hultman, L.; Sands, T. D. Dislocation-Pipe Diffusion in Nitride Superlattices Observed in Direct Atomic Resolution. *Sci. Rep.* **2017**, *7* (1), 46092.
(54) Schroeder, J. L.; Saha, B.; Garbrecht, M.; Schell, N.; Sands, T. D.; Birch, J. Thermal Stability of Epitaxial Cubic-TiN/(Al,Sc)N Metal/Semiconductor Superlattices. *J. Mater. Sci.* **2015**, *50* (8), 3200−3206.
(55) Chakraborty, S.; Uchiyama, H.; Garbrecht, M.; Bhatia, V.; Pillai, A. I. K.; Feser, J. P.; Adroja, D. T.; Langridge, S.; Saha, B. Phononic Bandgap and Phonon Anomalies in HfN and HfN/ScN Metal/Semiconductor Superlattices Measured with Inelastic x-Ray Scattering. *Appl. Phys. Lett.* **2020**, *117* (11), 111901.
(56) Gioti, M.; Arvanitidis, J.; Christofilos, D.; Chaudhuri, K.; Zorba, T.; Abadias, G.; Gall, D.; Shalaev, V. M.; Boltasseva, A.; Patsalas, P. Plasmonic and Phononic Properties of Epitaxial Conductive Transition Metal Nitrides. *J. Opt.* **2020**, *22* (8), 084001.
(57) Biswas, B.; Saha, B. Development of Semiconducting ScN. *Phys. Rev. Mater.* **2019**, *3* (2), 020301.
(58) Yang, X.; Liu, X.; Yu, S.; Gan, L.; Zhou, J.; Zeng, Y. Permittivity of Undoped Silicon in the Millimeter Wave Range. *Electronics* **2019**, *8* (8), 886.
(59) Maurya, K. C.; Biswas, B.; Garbrecht, M.; Saha, B. Wave-Vector-Dependent Raman Scattering from Coupled Plasmon−Longitudinal Optical Phonon Modes and Fano Resonance in n -type Scandium Nitride. *Phys. Status Solidi RRL* **2019**, *13* (9), 1900196.
(60) Wood, B.; Pendry, J. B.; Tsai, D. P. Directed Subwavelength Imaging Using a Layered Metal-Dielectric System. *Phys. Rev. B* **2006**, *74* (11), 115116.
(61) Krishnamoorthy, H. N. S.; Jacob, Z.; Narimanov, E.; Kretzschmar, I.; Menon, V. M. Topological Transitions in Metamaterials. *Science.* **2012**, *336* (6078), 205−209.
(62) Guler, U.; Boltasseva, A.; Shalaev, V. M. Refractory Plasmonics. *Science.* **2014**, *344* (6181), 263−264.
(63) Yu, S.; Wilson, A. J.; Kumari, G.; Zhang, X.; Jain, P. K. Opportunities and Challenges of Solar-Energy-Driven Carbon Dioxide to Fuel Conversion with Plasmonic Catalysts. *ACS Energy Lett.* **2017**, *2* (9), 2058−2070.
(64) Tadepalli, S.; Slocik, J. M.; Gupta, M. K.; Naik, R. R.; Singamaneni, S. Bio-Optics and Bio-Inspired Optical Materials. *Chem. Rev.* **2017**, *117* (20), 12705−12763.
(65) Chen, T.-A.; Un, I.-W.; Wei, C.-C.; Lu, Y.-J.; Tsai, D. P.; Yen, T.-J. Alternating Nanolayers of Dielectric MgF 2 and Metallic Ag as Hyperbolic Metamaterials: Probing Surface States and Optical Topological Phase Transition and Implications for Sensing Applications. *ACS Appl. Nano Mater.* **2021**, *4* (2), 2211−2217.
(66) Ma, Q.; Qian, H.; Montoya, S.; Bao, W.; Ferrari, L.; Hu, H.; Khan, E.; Wang, Y.; Fullerton, E. E.; Narimanov, E. E.; Zhang, X.; Liu, Z. Experimental Demonstration of Hyperbolic Metamaterial Assisted Illumination Nanoscopy. *ACS Nano* **2018**, *12* (11), 11316−11322.
(67) Chang, Y.-C.; Liu, C.-H.; Liu, C.-H.; Zhang, S.; Marder, S. R.; Narimanov, E. E.; Zhong, Z.; Norris, T. B. Realization of Mid-Infrared Graphene Hyperbolic Metamaterials. *Nat. Commun.* **2016**, *7* (1), 10568.
(68) Tumkur, T.; Barnakov, Y.; Kee, S. T.; Noginov, M. A.; Liberman, V. Permittivity Evaluation of Multilayered Hyperbolic Metamaterials: Ellipsometry vs. Reflectometry. *J. Appl. Phys.* **2015**, *117* (10), 103104.
(69) Belyi, V.; Kurilkina, S.; Kazak, N.; Agabekov, V. Surface Plasmon-Polaritons and Transverse Spin Angular Momentum at the Boundary of Hyperbolic Metamaterial with Arbitrary Orientation of the Optical Axis. *Adv. Electromagn.* **2017**, *6* (3), 70.
(70) Sreekanth, K. V.; De Luca, A.; Strangi, G. Experimental Demonstration of Surface and Bulk Plasmon Polaritons in Hypergratings. *Sci. Rep.* **2013**, *3* (1), 3291.
(71) Korobkin, D.; Neuner, B.; Fietz, C.; Jegenyes, N.; Ferro, G.; Shvets, G. Measurements of the Negative Refractive Index of Sub-Diffraction Waves Propagating in an Indefinite Permittivity Medium. *Opt. Express* **2010**, *18* (22), 22734.
(72) Feng, K.; Sivco, D.; Hoffman, A. J. Nanoscale Hyperbolic Metamaterial Resonators in Semiconductors. In *Conference on Lasers and Electro-Optics*; OSA: Washington, DC, 2016; *Vol. 1*, p FTh4D.2. DOI: 10.1364/CLEO_QELS.2016.FTh4D.2.
(73) Ishii, S.; Kildishev, A. V.; Narimanov, E.; Shalaev, V. M.; Drachev, V. P. Sub-Wavelength Interference Pattern from Volume Plasmon Polaritons in a Hyperbolic Medium. *Laser Photon. Rev.* **2013**, *7* (2), 265−271.
(74) Naik, G. V.; Liu, J.; Kildishev, A. V.; Shalaev, V. M.; Boltasseva, A. Demonstration of Al:ZnO as a Plasmonic Component for near-Infrared Metamaterials. *Proc. Natl. Acad. Sci. U. S. A.* **2012**, *109* (23), 8834−8838.

https://doi.org/10.1021/acsaem.1c03467
ACS Appl. Energy Mater. XXXX, XXX, XXX−XXX